ELSEVIER

Contents lists available at ScienceDirect

# Biosensors and Bioelectronics

journal homepage: www.elsevier.com/locate/bios





# Redox-mediated Biomolecular information transfer in single electrogenetic biological cells

Daniel Kaufman<sup>a</sup>, Chen-Yu Chen<sup>b</sup>, Chen-Yu Tsao<sup>b</sup>, Zhiling Zhao<sup>b</sup>, Avia Lavon<sup>a</sup>, Gregory F. Payne<sup>b</sup>, William E. Bentley<sup>b</sup>, Hadar Ben-Yoav<sup>a,\*</sup>

- <sup>a</sup> Nanobioelectronics Laboratory (NBEL), Department of Biomedical Engineering and Ilse Katz Institute for Nanoscale Science and Technology, Ben-Gurion University of the Neevy, Beer-Sheva, 8410501, Israel
- <sup>b</sup> Institute for Bioscience and Biotechnology Research, University of Maryland, College Park, MD, 20742, United States

#### ARTICLE INFO

Keywords:
Bio-microelectromechanical systems (bio-MEMS)
Redox signaling
Electrogenetics
Single cell analysis
Lab on a chip
Bioelectrochemistry

#### ABSTRACT

Electronic communication in natural systems makes use, inter alia, of molecular transmission, where electron transfer occurs within networks of redox reactions, which play a vital role in many physiological systems. In view of the limited understanding of redox signaling, we developed an approach and an electrochemical-optical labon-a-chip to observe cellular responses in localized redox environments. The developed fluidic micro-system uses electrogenetic bacteria in which a cellular response is activated to electrically and chemically induced stimulations. Specifically, controlled environments for the cells are created by using microelectrodes to generate spatiotemporal redox gradients. The in-situ cellular responses at both single-cell and population levels are monitored by optical microscopy. The elicited electrogenetic fluorescence intensities after 210 min in response to electrochemical and chemical activation were  $1.3 \times 10^8 \pm 0.30 \times 10^8$  arbitrary units (A.U.) and  $1.2 \times 10^8 \pm 0.30$  $\times$  10<sup>8</sup> A.U. per cell population, respectively, and 1.05  $\pm$  0.01 A.U. and 1.05  $\pm$  0.01 A.U. per-cell, respectively. We demonstrated that redox molecules' mass transfer between the electrode and cells - and not the applied electrical field - activated the electrogenetic cells. Specifically, we found an oriented amplified electrogenetic response on the charged electrodes' downstream side, which was determined by the location of the stimulating electrodes and the flow profile. We then focused on the cellular responses and observed distinct subpopulations that were attributed to electrochemical rather than chemical stimulation, with the distance between the cells and the stimulating electrode being the main determinant. These observations provide a comprehensive understanding of the mechanisms by which diffusible redox mediators serve as electron shuttles, imposing context and activating electrogenetic responses.

#### 1. Introduction

Ion-based physiological electrical communication, which is the main electrical signaling pathway (such as the neuromuscular system) in the human body, has been well researched and well demonstrated (Cuomo et al., 2015; Veeraraghavan et al., 2017). Early neurobiologists employed electrodes to measure action potentials, which constitute the basis of ion-driven electrical communication in biological systems (Cuomo et al., 2015; Hodgkin and Huxley, 1939). Instruments designed for reading ionic signals, such as the electrocardiogram (ECG) and the electroencephalogram (EEG), utilize an array of electrodes to capture these electrical activities, thus creating distinct and reliable patterns that facilitate the analysis of intricate biological systems (Buzsáki et al.,

2012; Crawford and Doherty, 2012; Misulis and Abou-Khalil, 2022; Noble et al., 2010). In addition to ionic electrical signaling, biological systems utilize electrical communication via electron transfer between biomolecules (McCord, 2016; Mohrin, 2021; Fridovich, 2016). This redox electrical pathway plays a vital role in various physiological systems. One example is the immune system, where immune cells release reactive oxygen species (ROS) toward target cells or tissues (Mohrin, 2021; Stephens et al., 2019). Another well-known system that uses the redox modality occurs in the microbiome, where several quorum sensing species rely on redox fluxes and oxidative gradients within the mucosal layer to maintain stable communication with neighboring bacteria (Homolak, 2023).

Although ion-based modalities (Fig. 1a) have been well studied and

E-mail address: benyoav@bgu.ac.il (H. Ben-Yoav).

 $<sup>^{\</sup>ast}$  Corresponding author.

are in use in various technologies, redox-signaling-based biological communication (Fig. 1b) is not well understood. The redox modality, which transfers electrons between biomolecules, is more difficult to monitor. Electrons do not exist as such in water and must be carried by a diffusible mediator. Yet, measuring these mediators and their redox state can be difficult, as redox involves electron transfer, which can be mutually affected by concurrently occurring molecular changes. In parallel, redox processes can also be affected by an external electric field.(Liu et al., 2017b). Electrochemistry offers methods to assess redox processes, allowing precise control over electrode surface potentials and charge (Perez, 2016). To leverage these methods to enable information transfer between electronic and biological systems, chemical and biochemical electron carriers, commonly known as redox mediators, are used, resulting in redox-based electrogenetic communication (Li et al., 2017; Liu et al., 2017a, 2017b; Zhao et al., 2021). Indeed, it has been previously shown that in complex chemicals and biological systems electrochemical signaling in the presence of redox mediators exerts temporal control of the cellular response due to the far distance of the mediators from the electrode (Fig. 1c, top); examples of such chemical compounds are catechol (Kim et al., 2017; Wu et al., 2021), the insoluble fraction extracted from clove (Lee et al., 2014), and thiolated polyethylene glycol (PEG-SH) (Li et al., 2022), and biological examples are engineered Pseudomonas aeruginosa (Kim et al., 2013), and synthetic and engineered Escherichia coli cells (McKay et al., 2017; Stephens et al., 2019; Tschirhart et al., 2017; Vanarsdale et al., 2019; Virgile et al., 2018). In contrast, spatiotemporal control of cellular behavior can be obtained by harnessing the interface near the electrode to produce a heterogeneously distributed environment (Fig. 1c, bottom). Furthermore, despite the promising potential of redox-based electrogenetic communication, the fundamental physicochemical mechanism controlling the activation of single biological cells by the electrodes has not been elucidated. Importantly, a basic question has yet to be answered (Fig. 1d): Is the cell's electrogenetic activation due to the redox molecules' mass transfer between the electrode and the cell or is it due to the electrical field generated by the externally applied potential to the electrode?

To address this fundamental question, we developed a novel bioelectronic device, namely, a bi-modal electrochemical-optical lab-on-achip (EO-LOC) micro-system. This device is designed to activate and analyze the fluorescent responses of single electrogenetic bacterial cells in a spatiotemporally controlled manner (as opposed to the homogeneous input demonstrated so far) (Fig. 1e and f). With this set-up, we observed, for the first time, a significant difference in the responses of single cells, regardless of whether they were subjected to spatiotemporally controlled (heterogeneously distributed environment) or temporally controlled (homogeneously distributed environment) activation. Moreover, when testing the spatial effect of the electrochemical signal, we observed increased gene expression around the electrode downstream of the channel, whereas chemical activation produced a uniform distribution. These results indicate that the redox-based electrogenetic activation was due to the redox mediators' mass transfer and not to the electrode's electrical field. Thus, using our EO-LOC system, we leveraged redox gradients to produce a controlled environment, in which we were able to observe different phenotypic responses to the cells and observed different phenotypic responses. To study the mass-transferbased cellular response, we developed a mathematical model for the redox activation mechanism, which indicated the following scenario: For electrochemical activation, we found a partitioning of physiological behaviors, implying that different subpopulations of cells exist within a culture that was presumed to be homogeneous. Interestingly, for chemical activation, parameter scattering indicated that there were no subpopulations, implying that the subpopulations obtained with electrochemical activation were separated mainly on the basis of responses to physicochemical processes outside of the cells, and hence a more "digital" genetic expression than a continuous function of context. Overall, our novel EO-LOC platform for investigating the activation of redox-responsive gene circuits in bacteria revealed differential responses to identical redox-active molecules depending on the spatiotemporal conditions imposed by the platform (namely, either spatial proximity of the cells to electrochemically stimulating oxidizing electrodes or chemical activation by oxidative species). Our platform will thus prove useful for further study of redox biology and the mechanisms that underpin redox-activated biological functions.

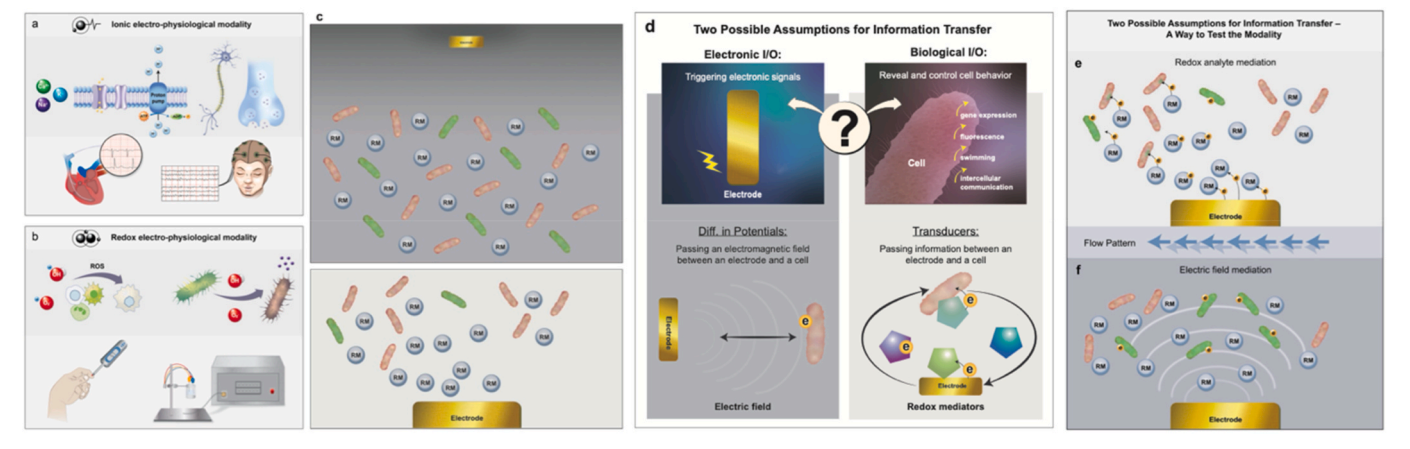


Fig. 1. (a) Ion-based physiological communication is the main electrical signaling pathway in the human body (e.g., ionic pumps and channels, and neuronal intercellular communication in the synapse), with the unique sensing (e.g., ECG and EEG) and actuating (e.g., pacemakers) instruments that are based on this pathway providing an interface between biology and electronics. (b) Despite accumulating knowledge on the vital role of redox molecules in various physiological systems (e.g., immune cell intercommunication via ROS and microbiome—host communication), redox-based physiological electrical communication remains difficult to understand, since there are only limited sensing and actuating instruments (e.g., glucometers and microelectrode platforms) available for investigating it. (c) Although redox-based electrical communication is temporally controlled and is achieved by using electrodes and redox mediators (RM), the cellular response occurs in a homogeneous environment (top), a limitation that can be overcome by performing the reaction in a heterogeneous environment (bottom), thereby enabling spatiotemporal control of the response by using redox gradients. (d) A bio-micro-systems approach may be used to investigate the two main hypotheses for electrode—cell electron transfer: the transduction of electrons by redox mediators or the movement of electrons caused by an externally applied electric field. (e) If the biological response is flow dependent, then the transfer of electrons is based on diffusible redox mediators, or (f) if the biological response is distributed radially, then the transfer of electrons is due to an electric field.

#### 2. Materials and methods

### 2.1. Chemicals, E. coli strain, and plasmids

Methanol (001368052100, Bio-Lab, Ltd.), calcium chloride (10195054, Alfa Aesar), hydrochloric acid (000846050100, Bio-Lab, Ltd.), sodium chloride (1259991, Merck), potassium hexacyanoferrate (II) trihydrate [Fcn(R); 1.04984.0100, Merck], potassium hexacyanoferrate(III) [Fcn(O); 1.04973.0100, Merck], pyocyanin from P.  $aeruginosa \geq 98\%$  (Pyo; p0046, Merck), acetone (376, Bio-Lab, Ltd.), hydrogen peroxide (1.07210.1000, Merck), potassium chloride (11595, Alfa Aesar), and 2-propanol (1301221, Bio-Lab) were used without further purification. Deionized water (DI; resistivity >18 M $\Omega$ ) was obtained from a Super Q water system (Millipore). Electrogenetic activation of E. coli DJ901 ( $\Delta$ lacU169,  $\Delta$ SoxRS901) for phiLOV expression by incorporating a pBR322 plasmid vector was performed as described previously (Tschirhart et al., 2017) and is presented in the Supplementary Information (section 1).

### 2.2. Multi-electrode array fabrication

Conventional microfabrication techniques, based on photolithography and thin film deposition, were used to fabricate gold microelectrodes on a glass substrate (prime grade, wafer diameter 100 mm, wafer thickness 500 µm, and double side polished, University Wafer), as follows. The glass substrate was cleaned with piranha solution (a 1:3 ratio mixture of hydrogen peroxide and sulfuric acid, HMxSquare SUSS MicroTec), dehydrated on a contact hot plate at 120 °C for 10 min, and left to cool at room temperature for 10 min. A TI xLift image reversal photoresist (Micro-Chemicals) was spin-coated (80RCDelta, Universal Spin-Coating system, SUSS MicroTec) onto the glass wafer (2200 rpm for 12 s at an acceleration rate of 800 rpm s $^{-1}$ ). The coated substrate was left on the spinner chamber for 5 min to settle, followed by a 'soft bake' step on the contact hot plate (110  $^{\circ}$ C for 2.5 min). The substrate was cooled to room temperature for 10 min and then exposed to a transparency mask (light flux of 7.6 mW cm<sup>-2</sup> for 65 s; Karl Suss Mask aligner MA6 system, SUSS MicroTec). A post-exposure bake was performed on the contact hot plate (120  $^{\circ}$ C for 2.5 min), and the substrate was left to cool to room temperature for 10 min. A flood exposure step was then performed (a light flux of 7.6 mW cm<sup>-2</sup>), and the exposed substrate was developed (AZ 726 MIF developer, Micro-Chemicals) for 6 min, rinsed with DI for 5 min, and dried with nitrogen gas following oxygen plasma cleaning for 0.5 min. Next, 20 nm-thick titanium and 300 nm-thick gold layers were evaporated onto the developed substrate using an E-gun deposition system (VST-TFDS-462 Service). The substrate was then submerged in acetone for 30 min, followed by rinsing with DI and drying with nitrogen gas. Optical images of the microfabricated microelectrodes were recorded using an optical microscope (MX-50A, Olympus). Finally, the microfabricated substrate was diced into single microchamber chips (Dicer ADT-7100, ADT). Prior to the electrochemical testing, the microfabricated chips were sequentially cleaned by rinsing with acetone, methanol, isopropanol, and DI to remove the organic residues, and then dried using nitrogen gas (Shukla et al., 2020).

#### 2.3. Microfluidic channel mold fabrication

Conventional microfabrication techniques, based on photolithography and thin film deposition, were used to fabricate a mold onto a silicon substrate (prime grade, wafer diameter 100 mm, wafer thickness 500  $\mu$ m, and double side polished, University Wafer). The silicon substrate was initially cleaned with piranha solution and dehydrated on a contact hot plate at 110 °C for 10 min. The cleaned substrate was left at room temperature for 10 min to cool. SU8-3050 negative photoresist (product no. 97, Micro-Chemicals) was spin-coated (80RCDelta, Universal Spin-Coating system, SUSS MicroTec) onto the silicon wafer (1000 rpm for 30 s at an acceleration of 300 rpm s  $^{-1}$ ). The coated

substrate was left on the spinner chamber for 5 min to settle, followed by a 'soft bake' step on the contact hot plate (95 °C for 45 min). Next, the substrate was cooled to room temperature for 10 min and then exposed to a transparency mask (a light flux of 7.6 mW cm $^{-2}$  for 50 s; Karl Suss Mask aligner MA6 system, SUSS MicroTec). A 'post-exposure bake' was performed on a contact hot plate (95 °C for 5 min), and the substrate was left to cool to room temperature for 10 min. The exposed substrate was developed [propylene glycol methyl ether acetate (PGMEA) developer, Micro-Chemicals] for 15 min, rinsed with DI for 5 min, and dried with nitrogen gas, followed by a 'hard bake' step on a contact hot plate (150 °C for 5 min). Finally, the substrate was cleaned with oxygen plasma for 2 min.

#### 2.4. Multi-electrode array and microfluidic channel bonding

We used a kit comprising an elastomer and a curing agent in a ratio of 10:1 (SYLGARD^TM 184 silicon kit, Dow) to prepare the PDMS mixture. After mixing the two components for 5 min, the PDMS was degassed in a vacuum bell. The degassed solution was poured onto the microfluidic channel mold and cured in an oven (80 °C for 40 min, with an acceleration rate of 4 °C min $^{-1}$ ). The cured PDMS was diced into single microchannel PDMS units. The multielectrode array and the PDMS microchannel units were placed in Diener Zepto-One Plasma Asher for 0.5 min using 67 W power in the presence of oxygen >95%, followed by attachment of the multielectrode array to the PDMS microchannel. The attached structure was left to stand overnight ( $\sim\!18$  h) for connection strengthening (Lee et al., 2016).

# 2.5. Bacterial incubation in the microfluidic channels and electrochemical activation

Following 2 h of growth in LB Miller broth, 1.5% w/v, *E. coli* (plasmid pT101, strain DJ901) cells were grown overnight in LB Miller broth, 1% w/v, in the presence of 1 mM ampicillin to an OD<sub>600</sub> of 0.2. Then, the bacteria were simultaneously streamed from 3 syringes (Harvard Apparatus Model 22 Syringe Pump) to the microfluidic channels (at a flow rate of 8  $\mu L$  min $^{-1}$ ) for 30 min. The solution inside the platform was allowed to stand for 1.5 h to enable the cells to attach to the glass. Thereafter, solutions containing the redox molecules and the LB broth were streamed into the microchannels (at a flow rate of 2  $\mu L$  min $^{-1}$ ) for 5 h. An oxidation potential of 0.5 V vs. a pseudo reference gold electrode (chronoamperometry technique) was applied using MultiPalmSens 4 (PalmSens) throughout the experiment to activate and measure the Fcn(O) reduction reaction (a chronoamperogram is presented in Fig. S1 and a correlation plot between the overall charge and the overall fluorescence is presented in Fig. S2).

### 2.6. Electrochemical measurements

All electrochemical measurements were performed using a Palm-Sens4 (Palmsens, Ltd.) and a three-electrode cell configuration consisting of the microfabricated Au electrodes (working electrode; 'WE', counter electrode; 'CE' and reference electrode; 'RE'). All electrodes were placed inside a microchannel (in chemical and electrochemical groups).

#### 2.7. Electrogenetic activation simulations

The numerical simulations, using the finite element method, for both the electrochemical reaction-diffusion model and the infusion-diffusion model, were performed using the Electroanalysis and the Laminar Flow modules, respectively, of the commercially available COMSOL Multiphysics software (version 5.6). The geometry and fluidic setup were defined based on the dimensions and parameters provided above. In the chemically induced model, the fluidic conditions were described by Navier-Stokes equations. In the electrochemical activation model, the

electrochemical reaction that defines Fcn(R)-Fcn(O) conversion was described by Butler-Volmer equations (Bard and Faulkner, 2001). The model describes the Poiseuille flow in the channel, the electron transfer between the electrode and the redox mediators, as well as the diffusion of Fcn(R) and Fcn(O) to and from the electrode surface. For our purposes, the two kinetic parameters,  $k_0$  and  $\alpha$ , were taken as 0.02 cm s $^{-1}$  and 0.5, respectively. The reference exchange current density was taken as 19,297 A m $^{-2}$ . The diffusion coefficients of Fcn(R) and Fcn(O) were both taken as  $7.3\times10^{-6}~{\rm cm}^2~{\rm s}^{-1}$ .

#### 2.8. Brightfield and fluorescent microscope imaging

Microscopy imaging was performed using a Nikon Eclipse Ti-2 inverted fluorescence microscope. Images were acquired using a Nikon CFI Plain Fluor  $10 \times$  objective and a 5.9 mega-pixel Nikon DS-Fi3 CMOS camera. Images were captured using two channels: brightfield with phase contrast and EGFP (Nikon C-FLL LFOV, 466/40 nm excitation, 525/50 nm emission, and a 495 nm dichroic mirror). Illumination for the brightfield imaging was provided by the built-in Ti-2E LED. Brightfield and GFP microscopic images were acquired every 30 min for 3.5 h to follow the bacterial responses to alterations in their environment. Epifluorescence excitation was performed using a 130-W mercury lamp (Nikon C-HGFI). Gain, exposure, and vertical offset were automatically determined using the built-in NIS functions to prevent user bias. Cells were imaged inside the electrochemical microfluidic channels' platform through the PDMS. An automated procedure was run on NIS, recording 264 images on each of the channels (24 locations, 8 for each microchannel, 11 timestamps - every 30 min). The images were exported from NIS format to a standard TIFF format using NIS-elements AR 5-10-01 software.

# 2.9. Cell population and single-cell image analysis

The microscope image data was cropped into small frames containing a small number of cells (1–5 each), and the intensity in each frame was divided by the number of cells in the corresponding brightfield image frame. The number of cells in the brightfield images was counted using threshold segmentation (0-6 cells in single cropped images), and the total intensity measured in the respective GFP image was calculated. The calculated intensity was divided by the number of cells. Consequently, the distribution of intensity for a single cell was obtained for each measured time and for each group (namely, electrochemically activated cells, chemically activated cells, and the control group). A Gaussian curve was fit to the histograms using the Python 3.8 'lmfit' package, and the mean intensity of a single cell was found for each time and group. The microscopic imaging and the electrochemical data were analyzed using Python (Spyder 5.0) and MATLAB. Six images in each tested group (in each microchannel) were observed. To detect the fluorescence in each image, the intensity of the whole fluorescent image was calculated. The image intensity at the beginning of the experiment was deducted from the signal in all the images to subtract the background noise and to track the fluorescent change in the bacteria. All the signals were set to a relative reference point of fluorescence (total light intensity equals zero). All the individual cell signals were set again to a relative reference point of fluorescence (mean light intensity equals zero). To analyze the upstream and downstream electrogenetic response, the microscopic images were first smoothed by a 30  $\times$  30 moving average window. Thereafter, the spatial response based on the location of the electrode in the channel was determined by evaluating the light intensity upstream and downstream of the electrode. Then, the fluorescence signal either upstream (left) or downstream (right) of the electrode in the chemical (Fig. S3d) and the electrochemical activation (Fig. S3e) groups was averaged. The analysis was followed by subtracting the initial background fluorescence captured in the images, thus normalizing the signal.

#### 3. Results and discussion

# 3.1. Electrochemical–optical lab-on-a-chip (EO-LOC) platform design, manufacture, and performance validation

To electrochemically control and optically observe the microenvironment around single bacteria and to electrochemically activate their responses, we addressed the following design considerations in the development of our EO-LOC device: (1) the ranges of the seed and growth capabilities of the bacteria under a constant flow of growth medium and the redox mediators, pyocyanin, Pyo(O) and ferricyanide, Fcn(O); (2) the spatial control of the electrochemical activation; and (3) the *in-situ* recording of the optical response of single cells. We addressed these considerations by developing an EO-LOC micro-system (Fig. 2) composed of two parts: (1) multiple microfluidic channels for the simultaneous handling of samples and (2) arrays of microelectrodes for the electrochemical activation of the cells.

We designed three parallel microfluidic channels (160  $\pm$  3 um in height and 1 mm in width) that enable the simultaneous performance of two electrochemical activation experiments (side channels) and one chemical activation experiment (the middle channel), wherein all experiments are performed with the same cells and identical media. Each electrochemical activation channel incorporates a microelectrode array that provides an electrochemical assessment. In addition, each electrochemical chamber comprises a row of eight gold disk working microelectrodes (50 µm radius) and a rectangular gold counter electrode (length = 12 mm, width = 0.2 mm) lying horizontally and at the same distance from each of the working microelectrodes (distance = 0.4 mm) (Fig. 2a). Conventional microfabrication techniques were used to fabricate the gold microelectrode array onto a glass substrate integrated with microfluidic channels and a platform that can be mounted under a microscope (Fig. 2b and c). The fluidic performance of the EO-LOC device was evaluated by allowing blue (middle channel) and red (side channels) dyes to flow through the microfluidic channels. We note that the dyes were spatially uniform throughout the channel (calculated Reynolds number = 0.064; calculations are shown in the Supplementary Information, section 2), and there were no signs of leakage (Fig. 2d).

The electrochemical performance of the EO-LOC device was characterized by using the commonly used redox couple Fcn(O)/Fcn(R). Cyclic voltammograms showed a reproducible electrochemical signal with reversible Nernstian characteristics (I\_{anodic peak} = 0.43  $\pm$  0.02  $\mu A;$  $I_{cathodic\ peak} = -0.41 \pm 0.01\ \mu\text{A};\ |I_{anodic\ peak}/I_{cathodic\ peak}| = 1.04 \pm 0.03;$  $E_{half\ peak} = 5.13 \pm 0.87$  mV). The results indicated robust electrochemical behavior and nearly identical electron transfer to and from each electrode in the same channel (Fig. 2e) [reproducibly within and between fabricated EO-LOCs was found, with low standard deviations for cyclic voltammogram signals in 4 replicates – standard error < 2.4% (Shukla et al., 2020)]. The small variability between the electrodes, which is positively related to the ionic resistance in the solution (Myland and Oldham, 2000), was due to the distance between the working and the pseudo-reference microelectrodes. Finally, the attachment of the electrogenetic bacteria to the bottom of the EO-LOC was validated (specifically, the study focused on the visible E. coli cells in the vicinity of the electrodes in the channel, whereas the cells on the surface of the electrode were not visible through the objective lens of the microscope) (Fig. 2f).

# 3.2. Response of populations and single E. coli cells to electrochemical and chemical activation

We started by studying the fluorescent response of single biological cells to the induction of a redox-based electrogenetic circuit. Specifically, oxidized pyocyanin, Pyo(O), and ferricyanide, Fcn(O), served to actuate and amplify the SoxRS oxidative stress regulon of *E. coli* that was used to activate the transcription and translation of the fluorescent reporter protein, phiLOV. Furthermore, the reduction within (Pyo(O)) or

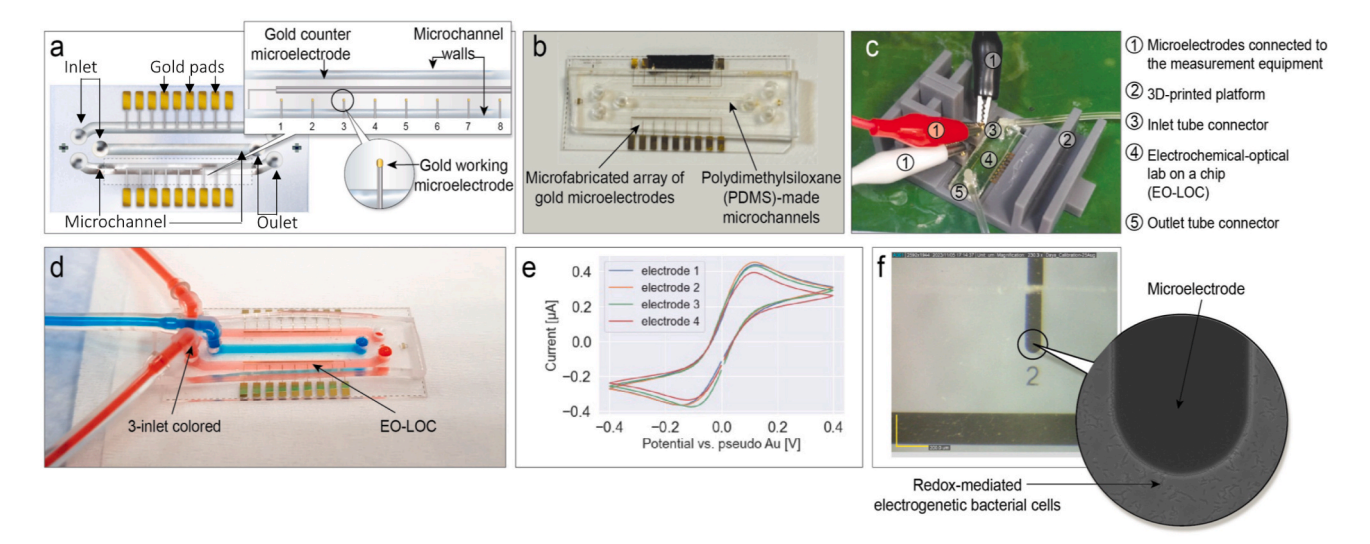


Fig. 2. Development of the electrochemical-optical lab-on-a-chip (EO-LOC) for spatiotemporal control of the cellular environment. (a) Top view of the EO-LOC, with two side channels for electrochemical actuation and the middle channel for a control group. The electrochemical channels consist of an electrochemical cell with eight individual working electrodes and a single counter electrode in the middle. (b) Photograph of the EO-LOC with three microchannels made of poly-dimethylsiloxane (PDMS). (c) Photograph of the EO-LOC assembled onto the fluorescent microscope in a 3D-printed holder. (d) Flow testing of the assembled EO-LOC; blue and red dyes flowing through the channels showed that there was no leakage. (e) The electrochemical validation of the microfabricated EO-LOC. Cyclic voltammograms of four electrodes show similar Nernstian-like behavior. (f) Microscope photograph of the fabricated electrode #2 and a close-up photograph of redox-mediated electrogenetic bacterial cells near the microelectrode (the study focused on the visible *E. coli* cells in the vicinity of the electrodes in the channel, whereas the cells on the surface of the electrode were not visible through the microscope's objective).

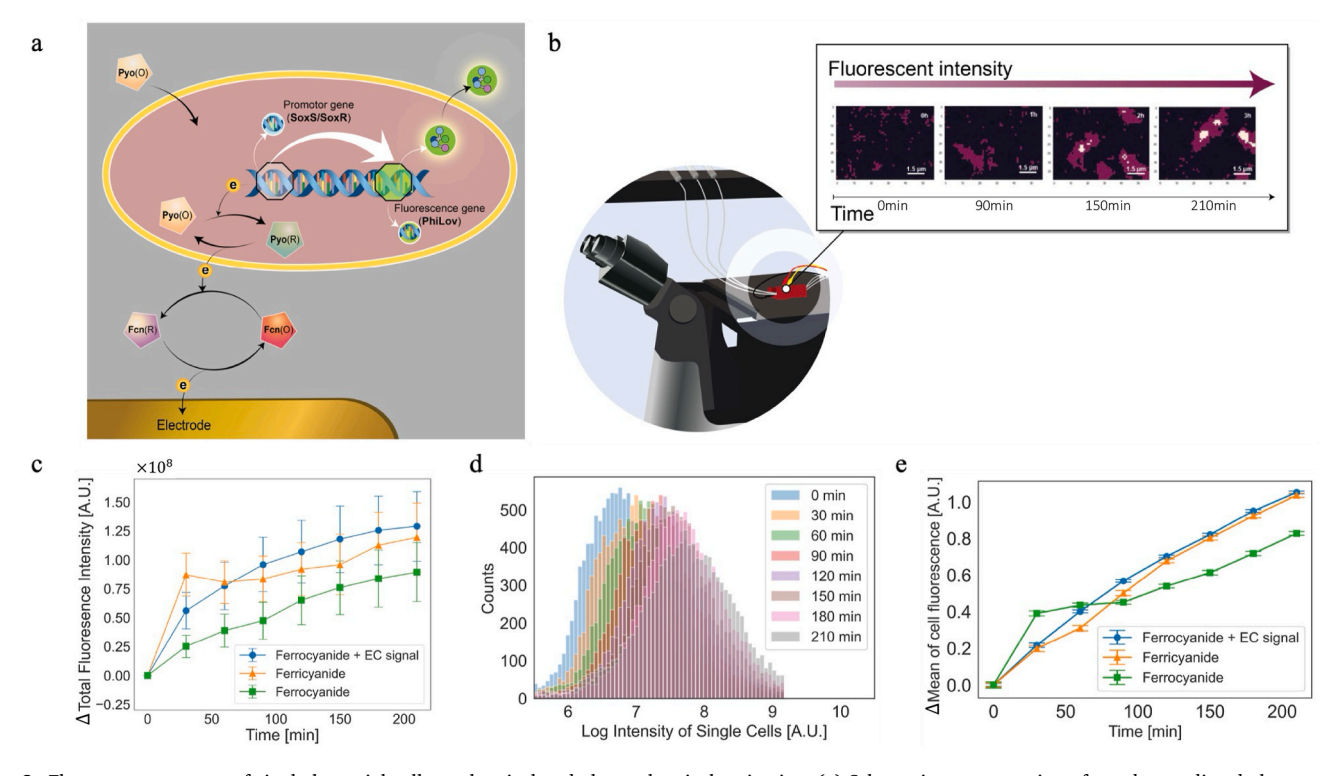


Fig. 3. Fluorescent response of single bacterial cells to chemical and electrochemical activation. (a) Schematic representation of a redox-mediated electrogenetic bacterial induction circuit for the fluorescent protein (phiLOV). The activation is enabled by the oxidation state of the redox mediator, which is controlled by the electrodes embedded within the bottom part of EO-LOC, oxidizing Fcn(R) to Fcn(O) near the cells. For chemical induction, the bacteria were exposed to either Pyo(O) or Fcn(O) to chemically activate the bacteria. (b) Fluorescent images of single cells following electrochemical activation for 0–3 h, showing increased fluorescence from single bacterial cells. (c) Total change in fluorescence intensity after 0, 30, 60, 90, 120, 150, 180, and 210 min in a cell population following either electrochemical (blue circles) or chemical (orange triangles) activation or no (green squares) activation. (d) Distribution of the fluorescence intensity after 0, 30, 60, 90, 120, 150, 180, and 210 min in single cells that were electrochemically activated. (e) Dependence of the change of mean fluorescence intensity from the single cell distribution analysis following electrochemical (blue circles), chemical (orange triangles), or no (green squares) activation after 0, 30, 60, 90, 120, 150, 180, and 210 min.

on (Fcn(O)) the cell's membrane and the subsequent reoxidation at the electrode surface (Fcn(R)) served to continuously elicit production of phiLOV (see Methods and Supplementary Information, section 1) as long as the electrochemical potential was applied to the electrode (Tschirhart, 2017). The induction was mediated by flow or by electrode-based activation of identical molecular signals (Pyo, Fcn) in both cases (Fig. 3a). Thus, for the electrochemical activation, the oxidation state of the redox mediator was controlled by the electrodes embedded in the bottom part of the EO-LOC device. The cellular fluorescent response was therefore activated by electro-oxidizing Fcn(R) to Fcn(O) near the cells. For chemical induction, the growth medium was supplemented with either Pyo(O) or Fcn(O). For electrochemical activation of the bacteria, Pyo(O) and Fcn(R) were used under an electrical potential, and for the control group Pyo(O) and Fcn(R) were added to the flow in the channel. In a preliminary experiment (Fig. S4), the optimal concentrations of the electrochemical mediators, Pyo and Fcn, were found to be  $2~\mu M$  and 8mM, respectively, under aerobic conditions. To analyze the fluorescent response of the cells, we acquired images from locations near six electrodes (for the control group, we acquired images at six random locations) (Fig. S5) and cropped the images into small sections containing between one and six cells (Fig. 3b and Fig. S7b). All three groups (chemically activated, electrochemically activated, and control) showed a steady increase in the fluorescent signal as time progressed. This was anticipated by chemical activation (Fcn(O)), electrochemical activation (Fcn(R)), and by spontaneous fluorescence and chemical activation (Fcn (R)) with oxygen as an oxidant, demonstrating increased synthesis of the fluorescent phiLOV protein (the electrogenetic activation technique is described in Supplementary Information, section 1) (Tschirhart et al., 2017). The cytotoxicity of Pyo and Fcn was evaluated by testing the E. coli fluorescent response to different concentrations of the redox mediators (Supplementary Information, section 5).

To determine the fluorescent response of the cells from the acquired images, the first step was to quantify the total fluorescent response of all the cells to chemical and electrochemical activations (Fig. 3c). The total fluorescence intensity values measured from the electrochemically and chemically activated groups increased faster than those of the control group throughout the experiments. After 90 min, the cumulative fluorescence intensity in the electrochemically activated group increased by  $0.96 \times 10^8 \pm 0.23 \times 10^8$  arbitrary units (A.U.) per cell population, whereas the fluorescence intensity in the chemically activated group increased by  $0.83 \times 10^8 \pm 0.20 \times 10^8$  A.U. per cell population and by  $0.47 \times 10^8 \pm 0.16 \times 10^8$  A.U. per cell population in the control group. The cumulative population fluorescence intensity increase was higher after 210 min, with the electrochemically and chemically activated groups increasing to  $1.3 \times 10^8 \pm 0.30 \times 10^8$  A.U. and  $1.2 \times 10^8 \pm 0.30$  $\times$  10<sup>8</sup> A.U. per cell population, respectively, and the control group increasing only to  $0.89 \times 10^8 \pm 0.26 \times 10^8$  A.U. per cell population. The differences between the population responses to electrochemical and chemical activation were found to be insignificant throughout the entire experiment ( $p_{value} < 0.11$ ) with respect to the temporal scale for average single-cell fluorescence intensity. In contrast, the fluorescent population in the control group displayed a significantly lower signal than the fluorescent populations in both activated groups ( $p_{value} = 0.03$  after the first 30 min,  $p_{value} < 0.01$  between 30 and 210 min). The fluorescent population in the chemical activation group exhibited a higher growth rate according to the single cell distribution analysis than that in the electrochemical group in the first 30 min. This difference may be due to a non-uniform distribution of the oxidation agent (Fcn(O)) in the first few minutes of the electric activation (high concentrations of oxidation agent near the electrode and low concentrations far from it). This finding might also suggest that the electrochemical activation generates an oxidation agent slowly (compared with the immediate response in the first 30 min of cells exposed directly to the oxidant).

The next step was to quantify the fluorescent response of single bacterial cells to chemical and electrochemical activation. Microscopic images obtained from single cells were analyzed to show the

fluorescence intensity distribution of single cells as a function of time. To reduce the skewness and to normalize the distribution results, the data were analyzed on a logarithmic scale (Fig. 3d) (the cell distribution on a linear scale is shown in Fig. S7). For durations longer than 100 min, the mean fluorescence intensity curves obtained from individual cell responses showed an overall increased fluorescence intensity in response to both electrochemical and chemical activation, compared with the mean fluorescence intensity values obtained for the control group (Fig. 3e). After 120 min, the mean fluorescence intensity per cell in the electrochemical activation group increased by 0.72  $\pm$  0.02 A.U., whereas in the chemically activated and control groups the mean fluorescence intensity increased by 0.70  $\pm$  0.01 A.U. and 0.57  $\pm$  0.02 A.U. per cell, respectively. After 210 min, the increase in the fluorescence intensity per cell in both activated groups was higher than that in the control group, with the activated groups increasing by 1.05  $\pm$  0.01 A.U. and the control group by  $0.82 \pm 0.02$  A.U. Robust results were obtained based on a large population of cells, and repeatable images were recorded from six working electrodes (the reproducibility of multiple electrodes is discussed in section S3 and is presented in Table S1 in the Supplementary Information). The chemically and electrochemically activated groups showed a similar increasing trend in fluorescence intensity throughout the experiment, whereas the control group showed a high increase in the first 30 min (0.40  $\pm$  0.02 A.U.) compared with both activation groups (0.20  $\pm$  0.01 A.U.) per cell, which later decreased, compared with the activated groups. These results led to the conclusion that the single-cell generation of the phiLOV protein is amplified by the presence (or generation) of an oxidation agent near the bacterial membrane. The smaller biological response in the first hour can perhaps be explained by an excessively high concentration of oxidative species. Under these conditions, cellular processes are likely to be directed to preserving basic cellular functions until the cells adapt to the changed redox environment. We note that the ability to observe a specific cell response - as is awarded by our platform - is crucial if we are to better understand cellular protein generation and how redox mediator molecules affect this process (Subramanian et al., 2014; Wax et al., 1970; Wieckol-Ryk et al., 2020).

# 3.3. Single E. coli cells are activated based on their spatial location

We investigated whether the electrogenetic activation of single *E. coli* cells is due to the redox molecules' mass transfer between the electrode and the cells or to the electrical field generated by the externally applied potential to the electrode. By monitoring the cells' response both upstream and downstream of the electrodes, we could decouple the two activation mechanisms (Fig. 4a). If electrogenetic activation is indeed dominated by redox mechanisms, then we would expect to observe an increased fluorescent response downstream rather than upstream of the electrodes. Alternatively, if the dominant activation mechanism is the electrical field generated by the electrode, then we would not expect to observe different responses upstream and downstream of the electrodes.

We thus investigated the fluorescent response of cells to Fcn(O) introduced into the system either directly or by electrochemical generation and subsequent radial diffusion [we note that the quantity of cells increased throughout the experiment (< $\sim$ 10%) with no significant detachment, as shown in Fig. S8]. To determine the spatial distribution of the redox mediator in the system, we modeled and simulated the access of Fcn(O) to the cells in the chemically and electrochemically induced groups (Fig. 4b). The simulation results showed distinct differences in the concentrations of the redox mediator downstream vs. upstream of the electrode, as opposed to similar concentration distributions on both sides of the electrode during chemical activation.

We then investigated the spatial distribution of the fluorescent response of the *E. coli* cells upstream and downstream of the electrode. After 30 min Fcn(O) had accumulated around individual electrodes, without much difference in the spatial distributions between the electrodes (especially for electrodes 2–6). We did not observe any clear trend

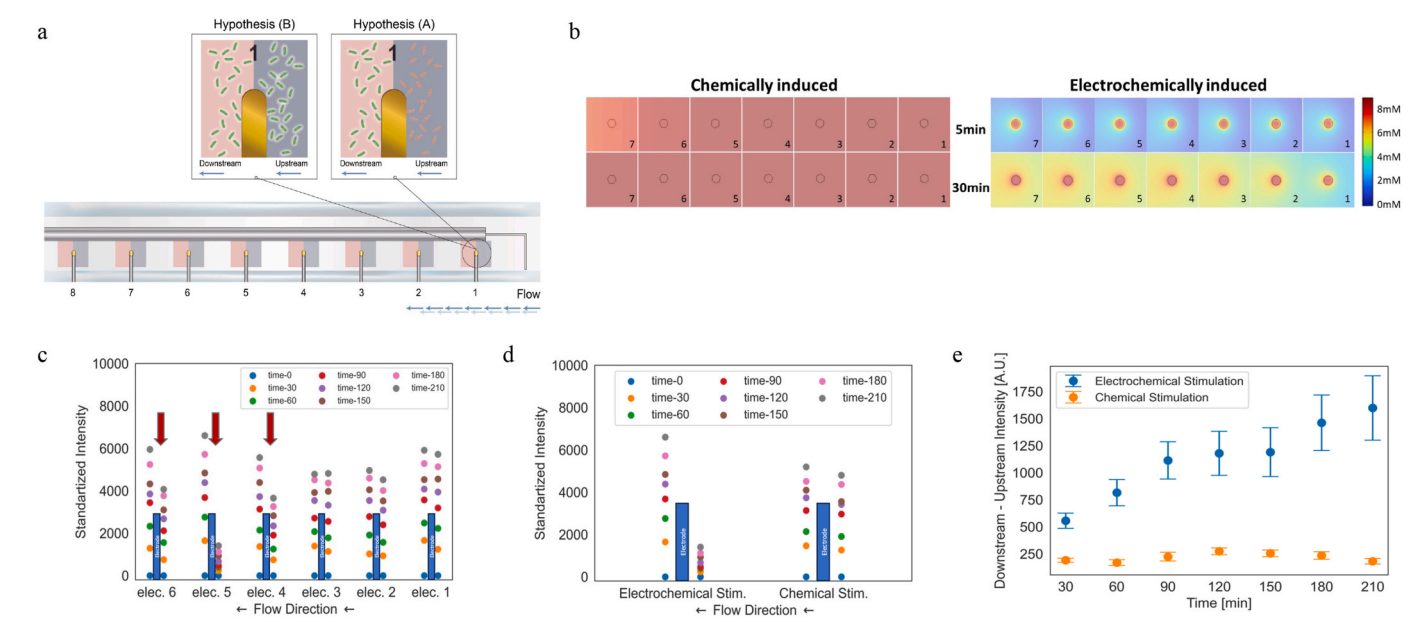


Fig. 4. Fluorescent response of the *E. coli* cells is dependent on their location with respect to the electrochemically activating electrodes and to the flow direction (i. e., upstream or downstream of the electrode). (a) Two main hypotheses were put forward for electrode–cell electron transfer: (A) electron transfer is based on the response of the cells to a diffusible redox molecular signal, and (B) the electron transfer derives from the response of the cells to the electrical field generated by the electrode. (b) Spatial concentration of Fcn(O) for chemically and electrochemically induced bacteria 5 and 30 min after activation [in the chemically induced group, the cells are exposed to the oxidative mediator by laminar flow, where Re = 0.064; in the electrochemically induced group, the oxidative mediator is generated by the electrode and diffuses radially to the cells. (c) Standardized fluorescence intensity generated from electrochemically activated bacteria that were either upstream or downstream of electrodes #1 to #6 at activation durations of 0–210 min. For the downstream electrodes (i.e., electrodes #4 to #6, denoted by red arrows), there was a higher difference in the fluorescence intensity upstream and downstream of the electrodes, suggesting a response to accumulated oxidative redox mediators. (d) Standardized fluorescence intensity generated by electrochemically or chemically activated bacteria that were either upstream or downstream of electrode #5 for activation durations of 0–210 min. (e) Ratio between downstream and upstream fluorescent responses averaged from all the electrodes for 30–210 min generated by either electrochemically activated (blue) bacteria.

in fluorescence intensity for the different electrodes in the channel; however, when we examined the fluorescence intensity near each electrode, we could see a clearer increase in fluorescence on the downstream side of electrodes #4, #5, and #6, which were located in the farthest part of the channel (Fig. 4c), than on the upstream side. Therefore, we suggest that there is a biological response to Fcn(O) species accumulating downstream of the channel that is compatible with the simulated distribution of the redox mediator shown in Fig. 4b; however, the concentration is stabilized at the distance between the electrodes, probably due to the mediator's reaction with the cells. The increase in the fluorescence intensity in the chemically activated group showed similar behavior. For example, for electrode #5 there was a uniform increase in fluorescence intensity on the upstream and downstream sides of the electrode, and the difference in the biological response was not significant, as opposed to the electrochemically stimulated bacteria (Fig. 4d).

Importantly, for the electrochemically activated bacteria, we observed an increase with time in the downstream/upstream fluorescence difference averaged from all the electrodes in the channel; such an increase was not found for the chemically activated bacteria (Fig. 4e). These results indicate the spatial ability of the device to control and monitor cell behavior using electrical activation. Furthermore, the results indicate that mass transfer of the redox mediators is the dominant electrogenetic activation mechanism and not to the electrical field generated by the electrode.

The importance of these results lies in the ability to show, for the first time, the spatiotemporal control of electrogenetic bacteria (the difference between upstream and downstream fluorescence intensity). Hence, this enabled imposing a context leading to a cellular response, thus enhancing our understanding of the biological responses to well-defined activation mechanisms.

# 3.4. Theoretical modeling of the redox-based electrogenetic activation indicated a different context for subpopulations of biological cells

A physicochemical model of the redox-based electrogenetic activation mechanism was developed. The first step was to model the biological response of the bacterial cells to electrochemical activation (Fig. 5a and b). Three dominant reactions were assumed: (1) intracellular Pyo(O) reduction at the promoter, which activates phiLOV gene transcription and the underlying translation to the phiLOV fluorescent protein, (2) Fcn(O) reduction at the membrane of the bacterial cell due to a redox pathway that originates from intracellular Pyo(R), and (3) electrochemical oxidation of Fcn(R) to Fcn(O) at the electrode surface. The continuous oxidation of Pyo(R) maintains and intensifies the fluorescent response of the phiLOV proteins. Several additional assumptions were also made, namely, the number of SoxR proteins and promoters is constant on a per cell basis; there is no turnover of phiLOV; there is no transport limitation for Pyo entry into the cells (Bhokisham et al., 2020; Motabar et al., 2021); and the individual cells' genetic circuits are identically activated under identical conditions. The resulting Markov chain is represented by equations (1) and (2):

$$\frac{d[Fcn(O)]}{dt} = -k_m[Fcn(O)] + k_o[Fcn(R)]$$
 (1)

$$\frac{d[phiLOV]}{dt} = k_{rx}[Fcn(O)]$$
 (2)

where Fcn(O) is the concentration [M] of the oxidized form, Fcn(R) is the concentration [M] of the reduced form, phiLOV is the concentration [M] of the phiLOV protein,  $k_o$  [s<sup>-1</sup>] is the electrochemical reduction heterogeneous electron transfer rate constant,  $k_m$  [s<sup>-1</sup>] is the chemical oxidation heterogeneous electron transfer rate constant at the membrane surface, and  $k_{rx}$  [s<sup>-1</sup>] is the production rate coefficient for the

 $log(k_{rx}) + logP_0$ 

#### Electrochemically activated Chemically activated a Z250 A 2000 1750 1750 Elnorescent Intensity [A.U.] 10 $\log(k_o + k_m)$ 1750 1750 0 1500 1250 -5 100 -2 -1 0 1 2 $log(k_m k_{rx}) + log P_0$ Time [min] b (Basal f log ( og , log 0

Fig. 5. Modeling the fluorescent response of single bacterial cells subjected to electrochemical and chemical activation. (a) Scheme of the Pyo-mediated redox cycle. (b) The scheme of the Fcn-mediated redox cycle. (c) For the electrochemical group, fitting of the model [phiLOV(t)] =  $P_0a_{EC}/b$  (t - 1/b exp(-bt)) + S; equation (3)] to the experimental average fluorescence intensity signal as a function of time. (d) For the electrochemical group, clustering of cells can be seen from a log-log plot of parameters in the model equation (3). (e) The log of the parameters from the model equation  $\{k_0 + k_m\}$  and the basal level  $\{S - P_0 k_0 k_{rx}/(k_0 + k_m)^2\}$ , and (f) the log of the parameters from the model equation  $\{P_0 k_0 k_{rx}\}$  and the basal response  $\{S - P_0 k_0 k_{rx}/(k_0 + k_m)^2\}$  parameters. (g) For the chemical group, fitting of the model [phiLOV(t)] =  $a_C t + S$ ; equation (4)] to the experimental average fluorescence intensity signal as a function of time. (h) The chemical group's clustering of the cells using the parameters from the model equation  $\{P_0 k_{rx}\}$  and the basal response (S) parameters. Log-log representation of the parameters representing individual cells. Clustering was performed using a Gaussian mixture model.

 $log(k_o + k_m)$ 

phiLOV protein, which incorporates multiple reactions (electron transfer between Pyo(R) and the membrane in the redox pathway; transcription of the phiLOV fluorescent gene; translation of RNA to the phiLOV protein; and the transfer of phiLOV protein to a fluorescent signal). In all cases, a constant flow in the channel, introducing a constant concentration of Pyo(O) and either Fcn(O) or Fcn(R), was assumed. In the chemically induced case, the cells were chemically activated, and as indicated in Fig. 4b, the flow was most likely uniform. In the electrochemically induced case, Fcn(R) was introduced and oxidized by the individual electrodes. Equations (1) and (2) resulted in the solution shown in equation (3):

$$[phiLOV(t)] = P_0 \frac{a_{EC}}{b} \left( t - \frac{1}{b} e^{-bt} \right) + S$$
 (3)

where  $a_{EC}=k_mk_{rx}$ ,  $b=k_o+k_m$ ,  $P_0$  - constant concentration of Fcn(O) species near the biological cell,  $S-\frac{P_0a_{EC}}{b^2}$  - basal level of the phiLOV protein (t = 0) , t [s] - time, and S [M] - a constant.

The next step was to measure the fluorescence response from single cells experimentally by applying the mathematical model in equation (3) (Fig. 5c); the following rate coefficients were calculated:  $k_0 = 0.99 \pm$ 0.14 [s<sup>-1</sup>],  $k_m = 0.99 \pm 0.14$  [s<sup>-1</sup>], and  $k_{rx} = 0.18 \pm 0.01$  [s<sup>-1</sup>]. Notably, the calculated rates suggested that the rates of reduction and oxidation of the mediator redox couple Fcn(O)/Fcn(R) are equal. This finding makes sense because the diffusion coefficients and the electrochemical properties of the two species constituting the redox couple are similar. The generation rate of the PhiLOV protein was found to be 5 times slower than the Fcn(O) inflow into the system, in agreement with the slow rates of biological responses, compared with the chemical/electrochemical reactions. We note that, in this study, the fluorescence intensity measured from the microscope images was analyzed, rather than the quantity of the fluorescent proteins (Gokhale and Gadgil, 2015; Winkler, 1995). Thus, it is important to emphasize that the calculated rates do not represent exact quantitative values, but, instead, represent a comparative analysis of the chemical/electrochemical activation in relation to the biological rates.

The following step was to apply the mathematical model (Eq. (3)) to

analyze the fluorescent response of single bacterial cells within a population. More specifically, we represented the fitted parameters,  $a_{EC}$  and b, and the basal response in 2D scatter plots (Fig. 5d-f). To better understand the physiological responses of the cells, we separated the parameters of the models and observed them individually and then combined them to obtain inferences. Interestingly, we observed three separate groups when the sum of  $k_o$  and  $k_m$  (i.e., the b parameter) is the main scattering factor. Thereafter, we used a Gaussian mixture model (GMM) algorithm (Everitt and Hand, 1981) to cluster the groups. This result suggests that the electron transfer from the electrode through the cell membrane and vice versa is the main clustering factor between the groups. Clustering of the groups according to the  $k_o + k_m$  parameter can be explained in terms of the different transfer rates of electrons on the cell membrane (i.e.,  $k_m$ ) and the various distances between the cells and the electrode (different distances for the redox mediators to travel;  $k_o$ ). The  $k_m k_{rx}$  (i.e., the  $a_{EC}$ ) parameter corresponds to the biological reaction rate; the wide distribution of this parameter reflects the diverse behaviors of individual bacteria (a range of 7 log cycles along the x-axis) (Fig. 5e-g).

As shown in Fig. 5d, for the electrochemical action, we observed decreased variability in the  $k_m k_{rx}$  axis for cells with high  $k_o + k_m$  values (green), compared with the middle group (denoted in orange). Such behavior can be explained by the faster chain of reactions of electron transfer through the membrane, which exhibits a relatively similar biological rate and a low "biological noise" dependency. Another reason for the variability between the clustered groups can be explained by the lack of electron acceptors near the cell or an impaired mechanism of electron transport through the membrane. Overall, the readily observable partitioning of cells based on the electrochemical model suggests a partitioning of physiological responses that accompany the electrochemical activation (parameter  $k_0 + k_m$ ). These clusters illustrate the ability of the platform to differentiate cell responses by their electrochemical and optical responses in a spatiotemporal domain.

We developed another mathematical model for the chemical activation mechanism due to the flow of oxidized mediators (i.e., the chemical model). For this model, we assumed (Fig. 5b) that: (1) intracellular Pyo(O) reduction at the promoter activates phiLOV gene

transcription and the underlying translation to the phiLOV fluorescent protein, (2) the Fcn(O) concentration is high throughout, which continuously activates the biological cells at a constant rate and concentration (supported by the simulation shown in the previous section), and (3) the Fcn(O) reduction occurs at the membrane of the bacterial cell by virtue of a redox pathway that originates from intracellular Pyo (O). All additional assumptions were similar to those for the electrochemical model. The resulting Markov chain is similar to equation (1), resulting in the solution shown in equation (4):

$$[phiLOV(t)] = a_C t + S \tag{4}$$

where  $a_C=P_0k_{rx}$ ,  $P_0$  - constant concentration of Fcn(O) species near the biological cell, S - basal level of the phiLOV protein (t = 0), t [s] – time, and S [M] - a constant.

We then fitted equation (4) to the average cell response in the chemically activated group (Fig. 5g) and represented the fitted parameters  $a_C$  and S in a 2D scatter plot. To better understand the physiological reaction of the cells, we separated the parameters of the models and observed them individually. Using a clustering technique for the chemically activated group similar to the one we used for the electrochemical activation, we did not find clearly separated clusters of cells (Fig. 5h). Thus, the lack of clustering meant that we could not leverage our simple model to enable subpopulation separation, which suggests that all the cells in the entire group responded similarly, in keeping with our original assumption of a homogeneous environment.

Thus, we suggest that the electrochemical activation resulted in a heterogeneous cellular response. This heterogeneous response cannot be explained by downstream/upstream differentiation, since the cells were similarly distributed in all three subpopulations (Figs. S9 and S10); rather, it can be explained by (1) the mass transfer mechanism of convection due to the flow in the channel, which was not incorporated into the model, (2) the various distances of the cells from the electrode, (3) the spontaneous generation of other redox-active molecules by the electrode (such as hydrogen peroxide), (4) the non-uniformity of the redox-active gradients causing the biological system to respond differently, and/or (5) the negative effects on the cells from contacting the charged electrode. Thus, we found distinct sets of cells having disparate phenotypes. For the chemical activation, we found no distinct subgrouping—rather, a large deviation from the mean, which might suggest intrinsic biological noise or heterogeneity in protein expression. This phenomenon was seemingly dampened in comparison to electrochemical stimulation.

#### 4. Conclusion

In this study, we investigated the spatiotemporal dynamics of redox-mediated electrogenetic activation of single biological cells and we elucidated the underlying electrogenetic mechanisms. By utilizing our integrated EO-LOC bio-micro-system platform, we manipulated redox molecules via electrochemical activation to examine the fluorescent response of individual cells to external stimulations. Notably, we observed, for the first time, significant variability in cellular responses to electrochemical and chemical activations. Specifically, we observed increased gene expression localized around the electrodes during the electrochemical stimulation, in contrast to uniform distribution under chemical stimulation. This disparity suggested that electrogenetic activation is driven primarily by the redox mediators' mass transfer rather than by the electrodes' electric field.

Our findings emphasize the potential use of spatiotemporal control over electrogenetic contexts, offering insights into monitoring and reducing biological variance. By monitoring the behavior of a bacterial culture simultaneously via electrochemical and optical techniques, we observed the direct impact of environmental cues on individual cells. In contrast to previous work, the current study demonstrates how the local cellular distribution relative to the stimulating electrode influences the

bacteria's electrogenetic responses. Furthermore, we explored the differential effects of chemical versus electrochemical stimulation, revealing distinct activation patterns and different cell behaviors. The dependence of such microscale reactions on the electrode interface shows the localized nature of electrochemical stimulation compared to chemical or physical methods.

Given the spatial efficiency of optical activation now available in optogenetics and the native biological communication modality of redox molecules, we can propose a synergy in integrating electrogenetic and optogenetic systems to guide biological behavior. Moreover, the observed spatial responses and effective cell clustering under electrochemical stimulation can be used for local and controlled drug delivery and disease treatment. Ultimately, we envision that our platform can advance research on redox-dependent biological environments, including applications in human physiology and organ-on-chip systems. By elucidating the intricate interplay between electrodes and cells on the microscale level, our work provides an approach to fine-tuning, manipulating, and monitoring of biological systems.

#### CRediT authorship contribution statement

Daniel Kaufman: Writing – original draft, Validation, Methodology, Conceptualization. Chen-Yu Chen: Visualization, Methodology, Investigation. Chen-Yu Tsao: Methodology. Zhiling Zhao: Methodology. Avia Lavon: Validation, Methodology. Gregory F. Payne: Writing – review & editing, Validation, Methodology. William E. Bentley: Writing – review & editing, Funding acquisition, Conceptualization. Hadar Ben-Yoav: Writing – review & editing, Writing – original draft, Supervision, Investigation, Funding acquisition, Conceptualization.

#### **Declaration of competing interest**

The authors declare that they have no known competing financial interests or personal relationships that could have appeared to influence the work reported in this paper.

# Data availability

Data will be made available on request.

# Acknowledgments

We thank the Ilse Katz Institute for Nanoscale Science & Technology and the Nano-Fabrication Center for the fabrication equipment and help with the fabrication process. We also wish to thank the Israel Innovation Authority (grant #75700) and the Kreitman School for Advanced Studies Doctoral Scholarship for funding this work. We also appreciate the support from the US National Science Foundation (MCB #2227598) and the Gordon and Betty Moore Foundation (#11395), both in support of W.E.B. and G.F.P.

### Appendix A. Supplementary data

Supplementary data to this article can be found online at https://doi. org/10.1016/j.bios.2024.116546.

#### References

Bard, Allen J., Faulkner, Larry R., 2001. Electrochemical Methods: Fundamentals and Applications, second ed., pp. 1–833. https://doi.org/10.1023/A:1021637209564
Bhokisham, N., VanArsdale, E., Stephens, K.T., Hauk, P., Payne, G.F., Bentley, W.E., 2020. Nat. Commun. 11 (1 11), 1–12. https://doi.org/10.1038/s41467-020-16249-

Buzsáki, G., Anastassiou, C.A., Koch, C., 2012. Nat. Rev. Neurosci. 13, 407–421. https://doi.org/10.1038/nrn3241.

Crawford, Jacqui, Doherty, Linda, 2012. Practical Aspects of ECG Recording 153.

- Cuomo, O., Vinciguerra, A., Cerullo, P., Anzilotti, S., Brancaccio, P., Bilo, L., Scorziello, A., Molinaro, P., Di Renzo, G., Pignataro, G., 2015. Front. Neurosci. 9 https://doi.org/10.3389/fnins.2015.00277.
- Everitt, B.S., Hand, D.J., 1981. Finite Mixture Distributions. https://doi.org/10.1007/ 978-94-009-5897-5
- Fridovich, I., 2016. Redox-active Therapeutics. https://doi.org/10.1007/978-3-319-30705-3 1.
- Gokhale, S., Gadgil, C., 2015. PLoS One 10 (12), 143867. https://doi.org/10.1371/journal.pone.0143867.
- Hodgkin, A.L., Huxley, A.F., 1939. Nature 144 (3651 144), 710–711. https://doi.org/ 10.1038/144710a0.
- Homolak, J., 2023. Biogerontology 24, 741–752. https://doi.org/10.1007/S10522-023-10049-8.
- Kim, E., Gordonov, T., Bentley, W.E., Payne, G.F., 2013. Anal. Chem. 85, 2102–2108. https://doi.org/10.1021/AC302703Y.
- Kim, E., Liu, Z., Liu, Y., Bentley, W.E., Payne, G.F., 2017. Biomimetics 2. https://doi.org/ 10.3390/biomimetics2030011.
- Lee, H., Koh, D., Xu, L., Row, S., Andreadis, S.T., Oh, K.W., 2016. Micromachines 7, 1–9. https://doi.org/10.3390/mi7100173.
- Lee, M.E., Kim, E., Liu, Y., March, J.C., Bentley, W.E., Payne, G.F., 2014. J. Agric. Food Chem. 62, 9760–9768. https://doi.org/10.1021/JF503479D.
- Li, J., Liu, Y., Kim, E., March, J.C., Bentley, W.E., Payne, G.F., 2017. Free Radic. Biol. Med. 105, 110–131. https://doi.org/10.1016/j.freeradbiomed.2016.12.029.
- Li, J., Zhao, Z., Kim, E., Rzasa, J.R., Zong, G., Wang, L.X., Bentley, W.E., Payne, G.F., 2022. iScience 25, 104548. https://doi.org/10.1016/j.isci.2022.104548.
- Liu, Y., Kim, E., Li, J., Kang, M., Bentley, W.E., Payne, G.F., 2017a. Nano Communication Networks 11, 76–89. https://doi.org/10.1016/j.nancom.2017.01.002.
- Liu, Y., Li, J., Tschirhart, T., Terrell, J.L., Kim, E., Tsao, C.-Y., Kelly, D.L., Bentley, W.E., Payne, G.F., Liu, B.Y., Li, J., 2017b. Adv. Healthcare Mater. 6, 1700789 https://doi. org/10.1002/adhm.201700789.
- McCord, J.M., 2016. Redox active Therapeutics. https://doi.org/10.1007/978-3-319-30705-3 2.
- McKay, R., Hauk, P., Wu, H.C., Pottash, A.E., Shang, W., Terrell, J., Payne, G.F., Bentley, W.E., 2017. Biotechnol. Bioeng. 114, 2883–2895. https://doi.org/10.1002/bit 26391
- Misulis, K.E., Abou-Khalil, B., 2022. Atlas of EEG, Seizure Semiology, and Management. https://doi.org/10.1093/med/9780197543023.001.0001.

- Mohrin, M., 2021. Free Radic. Biol. Med. 165, 38–53. https://doi.org/10.1016/j. freeradbiomed.2021.01.034.
- Motabar, D., Li, J., Payne, G.F., Bentley, W.E., 2021. Curr. Opin. Biotechnol. 71, 137–144. https://doi.org/10.1016/j.copbio.2021.07.017.
- Myland, J.C., Oldham, K.B., 2000. Anal. Chem. 72, 3972–3980. https://doi.org/
- Noble, D., O'rourke, B., Lakatta, E.G., Maltsev, V.A., Vinogradova, T.M., 2010. Circ. Res. 106, 659–673. https://doi.org/10.1161/circresaha.109.206078.
- Perez, N., 2016. Electrochemistry, 25–52. https://doi.org/10.1007/978-3-319-24847-9-2
- Shukla, R.P., Cazelles, R., Kelly, D.L., Ben-Yoav, H., 2020. Talanta 209, 120560. https://doi.org/10.1016/j.talanta.2019.120560.
- Stephens, K., Zargar, A., Emamian, M., Abutaleb, N., Choi, E., Quan, D.N., Payne, G., Bentley, W.E., 2019. Biotechnol. Prog. 35, e2881 https://doi.org/10.1002/ http://doi.org/10.1002/
- Subramanian, M., Goswami, M., Chakraborty, S., Jawali, N., 2014. Redox Biol. 2, 865–872. https://doi.org/10.1016/j.redox.2014.06.007.
- Tschirhart, T., Kim, E., Mckay, R., Ueda, H., Wu, H.C., Pottash, A.E., Zargar, A., Negrete, A., Shiloach, J., Payne, G.F., Bentley, W.E., 2017. Nat. Commun. 8, 1–11. https://doi.org/10.1038/ncomms14030.
- Vanarsdale, E., Tsao, C.Y., Liu, Y., Chen, C.Y., Payne, G.F., Bentley, W.E., 2019. ACS Sens. 4, 1180–1184. https://doi.org/10.1021/acssensors.9B00085.
- Veeraraghavan, R., Györke, S., Radwański, P.B., 2017. J. Physiol. 595, 3823–3834. https://doi.org/10.1113/JP273058.
- Virgile, C., Hauk, P., Wu, H.C., Shang, W., Tsao, C.Y., Payne, G.F., Bentley, W.E., 2018. PLoS One 13, e0196999. https://doi.org/10.1371/j.pone.0196999.
- Wax, R., Rosenberg, E., Kosower, N.S., Kosower, E.M., 1970. J. Bacteriol. 101, 1092–1093. https://doi.org/10.1128/jb.101.3.1092-1093.1970.
- Wieckol-Ryk, A., Białecka, B., Thomas, M., 2020. Water Air Soil Pollut. 231, 1–16. https://doi.org/10.1007/S11270-020-04824-3.
- Winkler, K., 1995. J. Electroanal. Chem. 388, 151–159. https://doi.org/10.1016/0022-0728(94)03847-V.
- Wu, S., Zhao, Z., Rzasa, J.R., Kim, E., Li, J., VanArsdale, E., Bentley, W.E., Shi, X., Payne, G.F., 2021. Adv. Funct. Mater. 31, 2007709 https://doi.org/10.1002/adfm.202007709.
- Zhao, Z., Ozcan, E.E., Vanarsdale, E., Li, J., Kim, E., Sandler, A.D., Kelly, D.L., Bentley, W.E., Payne, G.F., 2021. ACS Chem. Biol. 16, 1099–1110. https://doi.org/ 10.1021/acschembio.1C00267.